HIERARCHICALLY NANOCORAL REEFS-LIKE $ZnCo_2S_4$ DEPOSITED ON NI FOAM AS AN ELECTRODE MATERIAL FOR HIGH-PERFORMANCE BATTERY-TYPE SYMMETRIC SUPERCAPACITOR.

Elsaid, M. A.[*]; Sayed, A. Z.[†]; Ashmawy, A. M.[†§]; Hassan, A. A.[*]; Waheed, A. F.[*] and Mohamed, S. G.[‡§]

[*] Metallurgy Department, Nuclear Research Center (NRC), Egyptian Atomic Energy Authority (EAEA) Cairo, Egypt.

[†] Chemistry Department, Faculty of Science (boys), Al-Azhar University, 11884, Egypt .

[‡] Mining and Metallurgy Engineering Department, Tabbin Institute for Metallurgical Studies (TIMS), Tabbin, Helwan 109, Cairo 11421, Egypt.

[§] Corresponding authors Email: saadmohamed@tims.gov.eg (S. G. Mohamed), ashraf_ashmawy2002@azhar.edu.eg (Ashraf M. Ashmawy).

ABSTRACT

The target for developing electrode materials with unique architecture and tailored composition is essential for influencing their electrochemical properties. The innovative porous zinc cobalt sulfide ($ZnCo_2S_4$/ Ni foam (NF)) nanocoral reef-like structure supported by 3D NF is fabricated by the hydrothermal method. Here is an advanced electrode for supercapacitors (SCs), which demonstrates the notable electrochemical performance of the electrode in terms of the specific capacity of 2055.2 C g^{-1} (specific capacitance of 1957.4 F g^{-1}) at 1 A g^{-1} and excellent cyclic stability of 89.2% capacity retention and 98% coulombic efficiency after 5000 cycles. Furthermore, the battery-type symmetric supercapacitors based on ZCS/NF have an ultrahigh energy density of 39.1 Wh kg^{-1} at a power density of 1637 W kg^{-1} with excellent cyclic stability, 93.3% capacity retention, and 100% coulombic efficiency after 6000 cycles. The outstanding characteristics can be attributed to the synergistic contribution of the $ZnCo_2S_4$/NF coral reef hierarchical architecture and the bimetallic sulfide with great valence states for rich redox reactions. Therefore, the nano coral reef $ZnCo_2S_4$/NF is promising electrode material for battery-type supercapacitors.

Keywords

Nanocoral reef like; Hydrothermal synthesis; Battery-type supercapacitor; $ZnCo_2S_4$.

1. INTRODUCTION

The need to develop new, higher-performance working electrodes for electrochemical devices with higher power/energy densities for more efficient use of renewable energy sources cannot be overstated [1-3]. Despite having larger energy densities, the currently overtaking Li-ion batteries disadvantage from lower power capabilities, owing to the intrinsic controlled character of both ionic diffusion and charge transfer inside the bulk electroactive electrodes [4-7]. Not only for its appealing electrochemical properties, but sustainable energy-based applications such as lithium-ion batteries, fuel cells, and supercapacitors (SCs) are also energy-based applications such as lithium-ion batteries, fuel cells, and supercapacitors (SCs) are currently being super-developed. SCs have a significant advantage over LiBs, including higher power densities, longer life spans, and fast charge-discharge abilities [8, 9]. Generally, Supercapacitors are classified according to storage mechanism into three types double-layered capacitors, pseudocapacitors, and

battery-type capacitors, based on their energy storage strategies [10-15]. Battery-type capacitors have a greater specific capacity due to the short ion diffusion length and interfacial influence that improves redox kinetics for matched electrode materials. As a result, battery-type electrode materials such as transition metal sulfides, hydroxides, oxides, and phosphides, selenide, among others, have received much attention [16-19]. Construction and fabrication of electroactive sources with particular construction and compositions have motivated a significant research study. Transition metal sulfides have long been studied as suitable faradaic electroactive electrodes attributed to their attractive electrochemical properties. This includes great valence states, excellent electrochemical conductivities, and activities. In particular, ternary metal sulfides MCo_2S_4 ($M=Ni^{2+}$, Mn^{2+}, Zn^{2+}, Fe^{2+} and Cu^{2+}) exert a synergistic effect on faradaic processes via incorporating one metal element [20, 21]. Furthermore, sulfur takes the place of oxygen, resulting in a much more flexible structure [22, 23]. Because of these concerns, MCo_2S_4 is likely to display higher electrochemical performances. Among these MCo_2S_4 electrode materials, $ZnCo_2S_4$ material has recently attracted rising attention and interest owing to its low cost, [24] nontoxicity, and excellent electrochemical performances in recent years [25]. Coral reef-like structures and electrode materials have combined advantages in electrochemical energy storage, which can effectively improve the interface areas between electrode and electrolyte and offer rich transfer channels for ions and electrons, leading to notable improvement of the electrochemical performances [26, 27].

Furthermore, significant research efforts have been focused on the synthesis of $ZnCo_2S_4$ nanostructures and the exploitation of their energy storage properties [28, 29]. Zinc-cobalt sulfide rhombic dodecahedral cages and $Zn_xCo_{3-x}S_4$ hollow tubular structures were successfully fabricated [30], and they similarly displayed high performances in energy storage [24]. Despite these advances, the design and synthesis of hollow $ZnCo_2S_4$ core-shell structures with desirable electrochemical performances are much fewer reported. Herein, the $ZnCo_2S_4$ nanocoral reef-like form is successfully synthesized on the NF as binder-free via an efficient hydrothermal method. The $ZnCo_2S_4$ nanocoral reefs perform as expected, with a high specific capacity of 2055.2 C g^{-1} at a current density of 1 A g^{-1} and just 10.8% loss, with 98% coulombic efficiency after 5000 charging-discharging cycles. Furthermore, a battery-type symmetric supercapacitor constructed of two electrodes $ZnCo_2S_4$/NF as cathode and anode provides specific energy of 39.1 Wh kg^{-1} at a power density of 1637 W kg^{-1} at the current density of 1 A g^{-1} and 93.3% capacity retention and 100% coulombic efficiency after 6000 cycles. The remarkable electrochemical performance of hollow $ZnCo_2S_4$ nanocoral reefs shows that they could be a promising candidate for energy storage.

2. EXPERIMENTAL SECTION

2.1. Materials

All the chemicals used in this study were analytical grade and were not purified further. Zinc nitrate hexahydrate ($Zn(NO_3)_2.6H_2O$, 98%), cobalt nitrate hexahydrate ($Co(NO_3)_2.6H_2O$, 99%), and sodium sulfide ($Na_2S.9H_2O$, 99.0%) were all provided by Sigma-Aldrich. In addition, urea ($CO(NH_2)_2$), Ammonium fluoride (NH_4F), potassium hydroxide (KOH), and absolute ethanol (C_2H_5OH) were obtained from Alfa Aesar. Nickel foam (NF) was purchased from MTI Korea. The NF (1 cm x 3 cm) was washed

with 3M HCl, ethanol, and deionized water to remove the surface contaminants and oxide layer.

2.2. Synthesis of $ZnCo_2S_4$ /NF

Inside a study, 2 mmol Zn $(NO_3)_2.6H_2O$, 4 mmol $Co(NO_3)_2.6H_2O$, 8 mmol NH_4F, and 10 mmol urea were dissolved in a mixed solution of 35 ml deionized water. Nickel foam (1 cm * 3 cm) was cleaned with acetone and a 3 M HCl solution to remove the oxide from the surface before being treated for 15 minutes with deionized water and absolute ethanol. The solution and clean Ni foam were then placed in a 50 mL Teflon-lined autoclave and heated for 12 h at 120 ºC. The resultant Ni foam was rinsed multiple times with deionized water and absolute ethanol before being dried at 60 ºC for 24 h to acquire the Ni precursor for producing $ZnCo_2S_4$. By exposing the precursor to a sulfurization procedure, the $ZnCo_2S_4$ was developed on Ni foam. The $ZnCo_2S_4$ precursor/Ni foam was heated for 12 hours at 160 ºC in a 50 mL Teflon-lined autoclave with 30 ml of 0.25 M Na_2S solutions. To obtain the $ZnCo_2S_4$ coral reef-like structure on Ni foam, the autoclave was cooled to room temperature, and the products were rinsed with deionized water several times before being dried at 60 ºC for 12 hours. The load of the active ingredient $ZnCo_2S_4$ on Ni foam is determined to be ~ 3 mg cm^{-2} based on the weight difference of Ni foam before and after the reaction.

2.3. Materials Characterization

The morphology and microstructure of the investigated electrodes were examined using field emission scanning electron microscopy (FE-SEM; ZEISS Germany) supported by energy-dispersive X-ray (EDX) elemental mapping. As well as transmission electron microscopy (TEM, FEI Tecnai G2F20) with an acceleration voltage of 200–103 V. An X-ray diffraction (XRD-6000, Shimadzu) technique utilizing CuK radiation was used to interpret the crystal structures of the samples. The electrodes' elemental compositions were also determined using (XPS) X-ray photoelectron spectroscopy using monochromatized AlK radiation (Thermo Scientific).

2.4. Electrochemical Investigations

The electrochemical performance of $ZnCo_2S_4$ growing on NF electrode for battery-type SCs was evaluated using a three-electrode system with $ZnCo_2S_4$/NF electrode as the working electrode, Ag/AgCl as the reference electrode, and a platinum plate as the counter electrode. Cyclic voltammetry (CV) curves were performed at several scan rates from 5 to 50 mV s^{-1} over a potential window of –0.8 to 0.9 V. Galvanostatic charge-discharge (GCD) tests were undertaken at various current densities ranging from 1 to 20 A g^{-1} over a potential window of −0.6 to 0.45 V. Electrochemical impedance spectroscopy (EIS) was conducted in the frequency range of 0.01 Hz to 100 kHz. All electrochemical measurements were performed using OrigaFlex-OGF01A (OrigaLys ElectroChem SAS, France) electrochemical workstation in a 6 M KOH solution. With equations (1) and (2), the specific capacitance and specific capacity are calculated in a specific method using GCD curves to determine discharge times [31, 32]:

$$C_s = 2\,\mathrm{I} \times \int \mathrm{Vdt}/(\,\mathrm{m} \times \Delta V^2) \quad (1)$$

$$C = 2\,I \times \int Vdt/(\,m \times \Delta V) \quad (2)$$

To design the symmetric battery-type SC cell, the $ZnFeNiCo_2S_4$/NF electrodes were used as both positive and negative. The specific energy (Wh kg^{-1}) and the specific power (W kg^{-1}) of the cell were calculated using equations (3) and (4) [33, 34].

$$E = I \times \int V dt / 3.6 \times m \quad (3)$$

$$P = 3600\, E/\Delta t \quad (4)$$

Where E is the specific energy, P is the specific power, and Δt is the discharge time.

3. Results and Discussion

3.1. XRD Investigation

To confirm the crystal structure of the prepared samples, high-quality XRD data were collected using a Bruker AXS X-ray diffractometer with Cu-Kα (λ=1.54056 A˚) radiation source in the 2θ range of 10-80° for each sample.

3.1.1. XRD investigation of $ZnCo_2S_4$/NF

XRD analysis was performed to survey the crystal structure of the obtained $ZnCo_2S_4$/NF. The diffraction peaks at 2θ of 31.2°, 37.9°, 50.1°, 55.3°, and 63.0° should be assigned to the (311), (400), (511), (440), and (620) lattice planes of $ZnCo_2S_4$ (JCPDS No. 20-0782) (figure 1) [35]. The peaks at 2θ of 44.6°, 52.1°, and 76.5° are ascribed to NF [36]. The impurity peak at 2θ of 21.9° corresponds to the Ni_3S_2 phase formed during the sulfidation treatment [37].

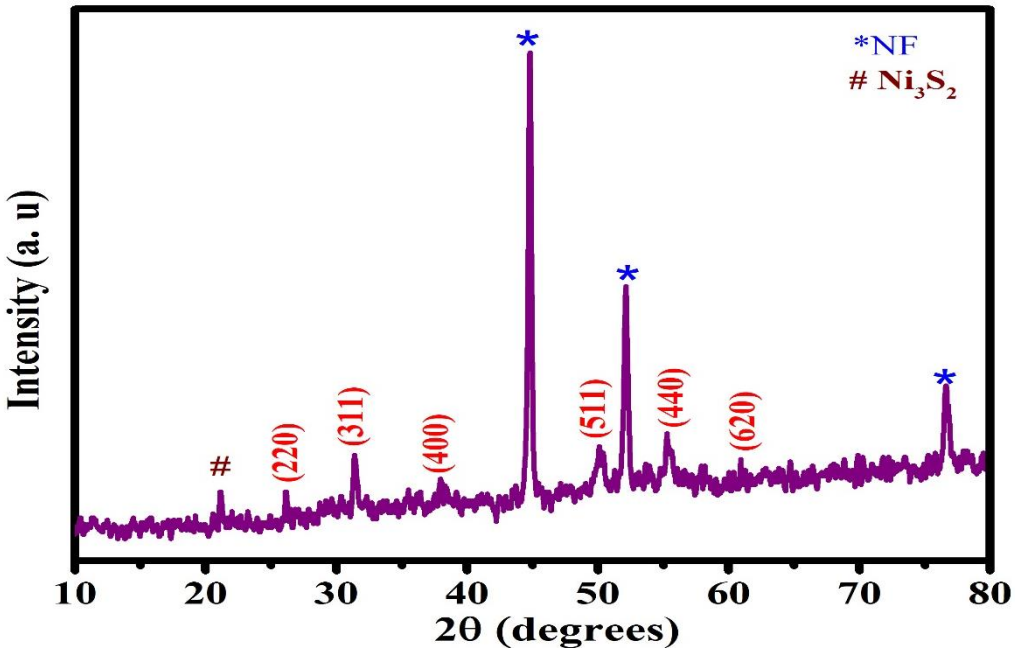

Fig. 1: XRD patterns of $ZnCo_2S_4$@NF.

3.2. X-ray Photoelectron Spectroscopic of $ZnCo_2S_4$/NF

The oxidation states and chemical composition of $ZnCo_2S_4$ were illustrated in figure 2 using XPS. Figure 2a displays the XPS spectrum survey, revealing the existence of O, C, S, Zn, and Co elements. The appearance of O 1s and C 1s peaks is attributed to exposing the sample to the air [38]. Peak deconvolution was performed using a Gaussian fitting method based on the Shirley background correction. Figure 2b displays the high-resolution spectrum of Zn 2p, in which two pronounced peaks appeared at binding energies of 1044.5 and 1021.5 eV, corresponding to Zn $2p_{1/2}$ and Zn $2p_{3/2}$, proving the presence of Zn^{2+} ion [39].

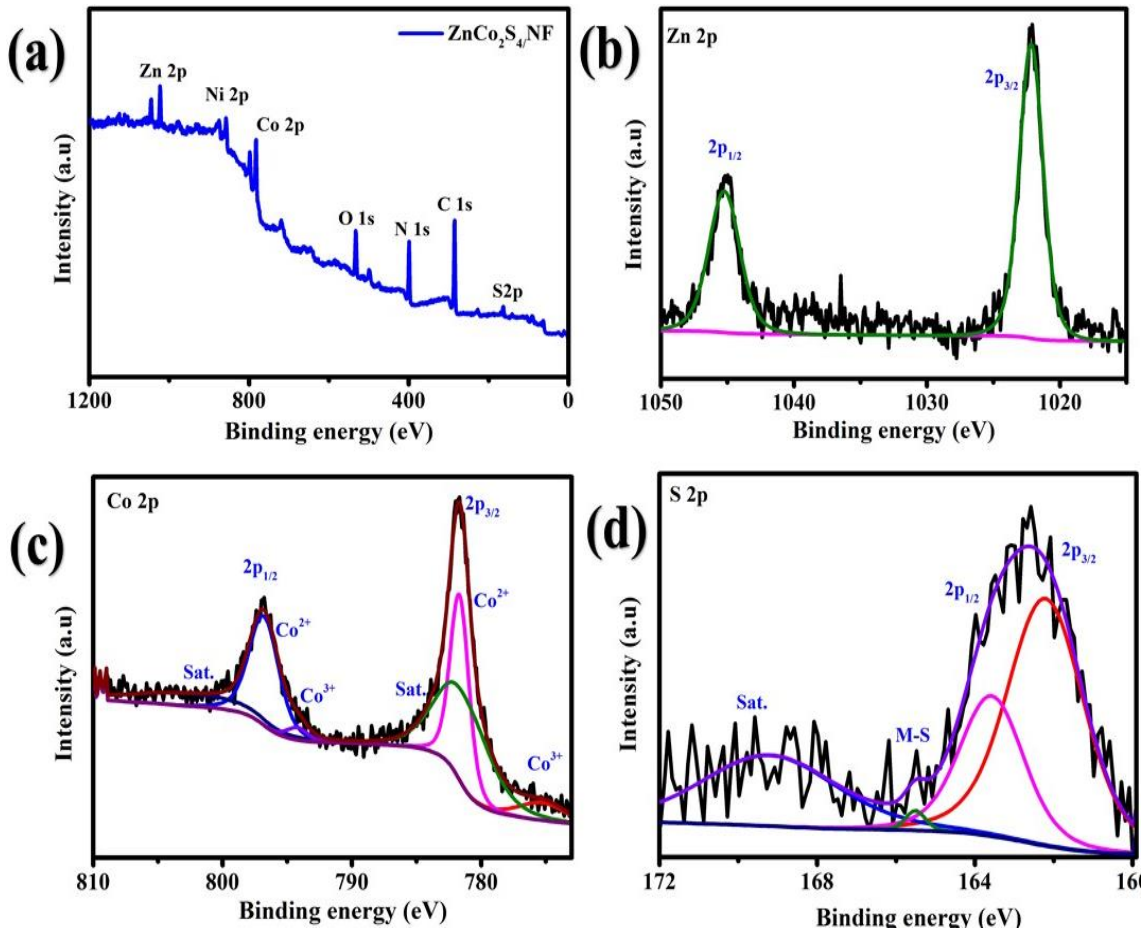

Fig. 2: XPS spectra of $ZnCo_2S_4$ on the NF: (a) survey spectrum, high resolution XPS spectra of (b) Zn 2p (c) Co 2p and(d) S 2p.

From the XPS results, the chemical composition of the $ZnCo_2S_4$ included Zn^{2+}, Co^{2+}, Co^{3+}, and S^{2-}. Figure 2c shows the high-resolution spectrum of Co 2p, which is deconvoluted into two satellites (denoted as "Sat") and two spin-orbit doublets, confirming the presence of both Co^{2+} and Co^{3+}. The peaks at binding energies of approximately 778.5 and 797.5 eV correspond to Co^{3+}, whereas the peaks at binding energies of 782 and 798.5 eV are attributed to Co^{2+} [37]. The high-resolution spectrum of S 2p (figure 2d) shows two peaks at 161 and 163 eV that are well assigned to S $2p_{1/2}$ and S $2p_{3/2}$, respectively [34], which can be set to metal–sulfur bonds. In contrast, the

satellite peak at 169 eV (sat.) was attributed to the surface-adsorbed oxidized sulfur species [32, 37].

3.3. Morphology and Microstructure Investigation

3.3.1. Morphology of $ZnCo_2S_4$/NF

The proper composition and uniform morphological assembly containing the porous structures are the critical parameters for affecting the electrochemical performance and facilitating the full utilization of electrode material. So, for investigating the nanostructures grown on the NF substrate, FESEM was carried out for $ZnCo_2S_4$ as depicted in figures 3a and 3b, respectively. The surface morphology of $ZnCo_2S_4$ shows the sponge coral reef-like structure. Further, higher magnifications of $ZnCo_2S_4$ have been performed for insight structural analysis of the sponge coral reef morphology, as shown in figures 3c and 3d. The higher magnification images show interconnected, overlapped sponge moss-like structures having tiny spike-like flowers. Thus, the unique form of composite $ZnCo_2S_4$ will provide a highly porous morphology, enhancing the specific relative surface area and increasing active sites for the adsorption of electrolyte ions during the faradaic reactions, implying the significant improved electrochemical performance of the electrode.

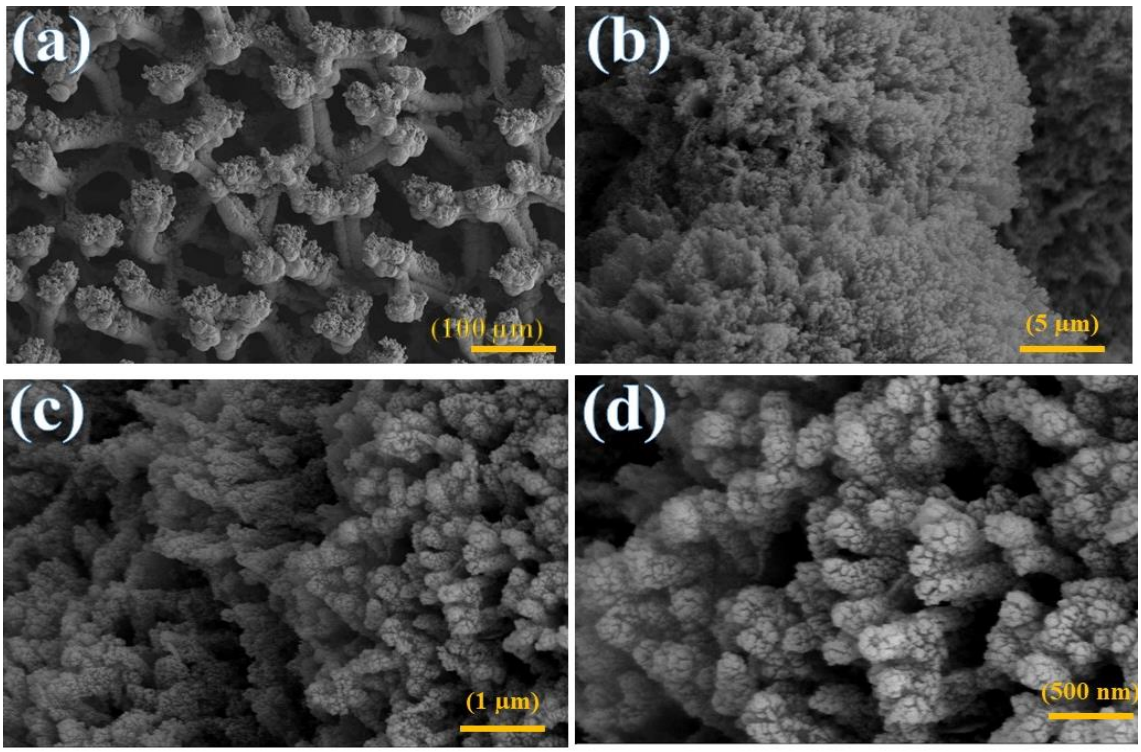

Fig. 3: FESEM images of (a- d) $ZnCo_2S_4$/NF at different magnifications.

EDS is also conducted to examine different constituent elements in the $ZnCo_2S_4$ scraped powder, as depicted in figure 4. The spectra corresponding to the Zn and Co and S ensure their existence in the structure. The TEM and HRTEM have been elucidated to observe the morphology and crystallinity of $ZnCo_2S_4$, as depicted in figures 5a to 5c. The obtained images are consistent with our HRSEM results. Figure 5d shows the SAED pattern of

materials. The diffusive rings in the SEAD pattern suggest the polycrystalline nature of the composite material. This agrees with the XRD results.

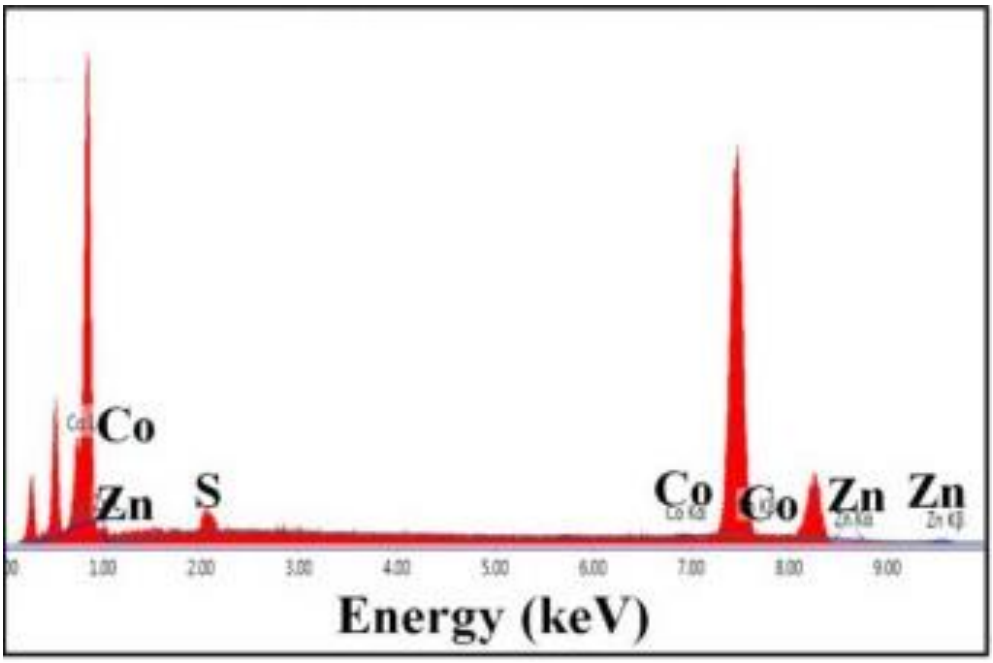

Fig. 4: The X-ray spectrometry (EDX) analysis of $ZnCo_2S_4$.

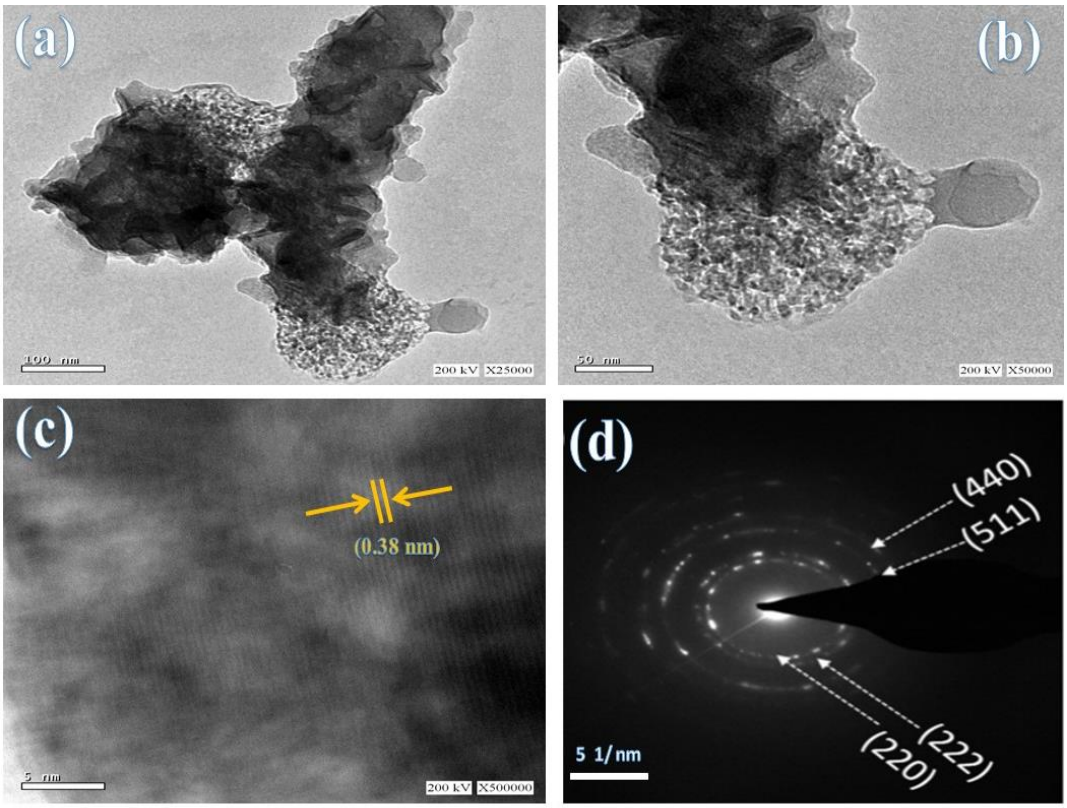

Fig. 5: (a-b) TEM image, and (c) HRTEM image of $ZnCo_2S_4$, nano coral reef, and (d) SAED pattern.

3.4. Electrochemical Measurements

3.4.1. Electrochemical performance of $ZnCo_2S_4$/NF nanocoral reef electrode materials.

The electrochemical performances of $ZnCo_2S_4$ nanocoral reef as supercapacitor material were determined on a three-electrode cell in a 6 M KOH electrolyte. Figure 6 illustrates the cyclic voltammograms (CV) of $ZnCo_2S_4$/NF, located at various scanning rates of 5–50 mV s^{-1} in the potential range of about -0.8–0.9 V a pair of long redox peaking's. The rectangular-quasi shape of the CV reveals participants of a significantly stronger faradic process in the energy storage characteristics-type of battery-based capacitors. Although all faradaic current increased at higher scan rates, significant shifts in peaking sites happen for all anodic and cathodic procedures (figure 6a). This shows that the redox procedures were well-control approaches without visible physical transportation at the electrode interfaces.

Furthermore, All CV curves contain a pair of redox peaks, revealing a quasi-reversible Faradaic redox reaction and a property of battery-like capacitors. The redox peaks could be assigned to the Faradaic reactions associated with Zn-S-OH and Co-S-OH [40]. The Faradaic response fulfils specific electrochemical performance and may be represented as:

$$ZnCo_2S_4 + 4OH^- \leftrightarrow ZnSOH + 2CoSOH + SOH^- + 3e^- \quad (5)$$

$$CoSOH + OH^- \leftrightarrow CoSO + H_2O + e^- \quad (6)$$

$$ZnSOH + OH^- \leftrightarrow ZnSO + H_2O + e^- \quad (7)$$

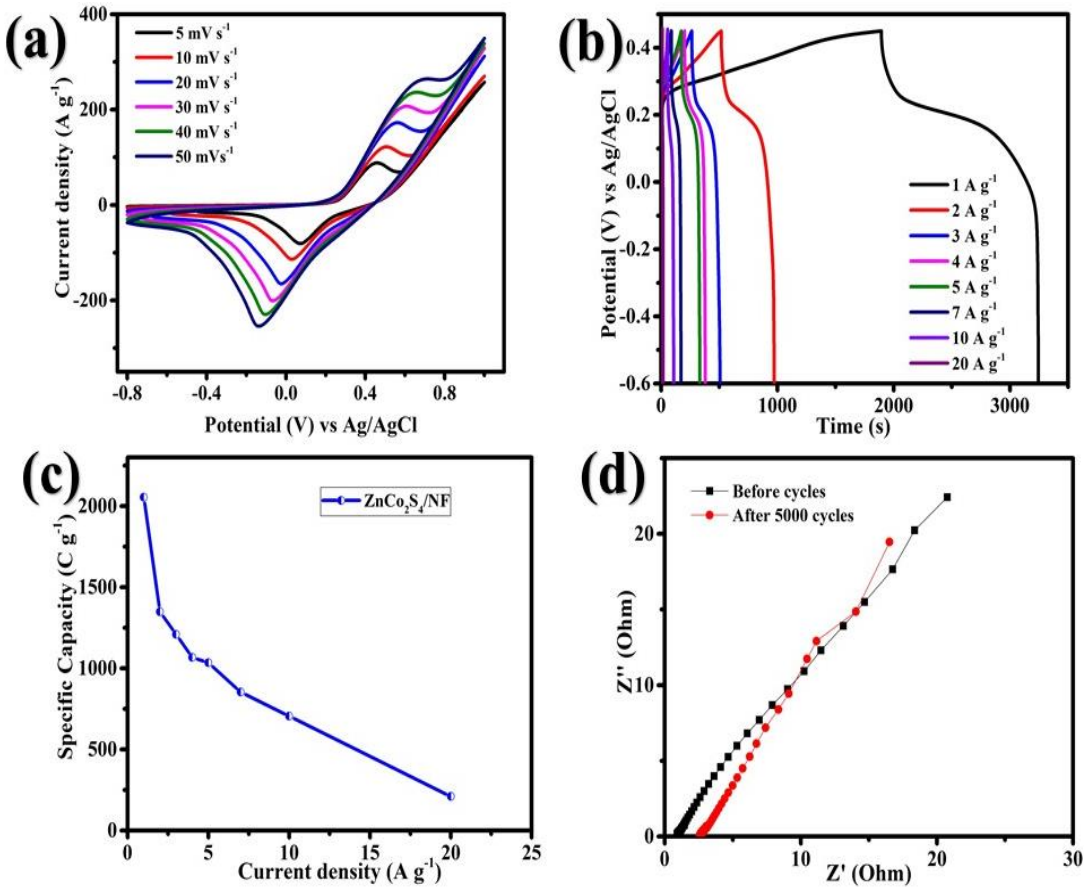

Fig. 6: (a) CV curves of $ZnCo_2S_4$/NF at various scan rates, (b) GCD curves $ZnCo_2S_4$/NF at various current densities, (c) the specific capacities of $ZnCo_2S_4$/NF at various current densities, (d) ESI $ZnCo_2S_4$/NF before and after 5000 cyclic stability.

Furthermore, GCD evaluations were carried out at various current densities within the voltage ranges of 0–0.45 V at current values ranging from 1 to 20 A g^{-1}, as shown in figure 6b. The battery-based features of $ZnCo_2S_4$/NF are confirmed by distinct voltage plateaus in the charge plot at reduced current densities, as shown in figure 6b. By displaying well-being linear sloping and symmetry, the triangular-type charge/discharge graphs reveal the excellent electrochemical activities of $ZnCo_2S_4$/NF. The GCD curves of the $ZnCo_2S_4$/NF sample have been assigned at various current densities. The GCD curves of the $ZnCo_2S_4$/NF sample were posted at different current densities. The specific capacity was calculated using the following equations based on the discharge duration results of GCD.

The specific capacity of the $ZnCo_2S_4$/NF electrode was calculated using equation (2). The specific capacities versus current densities are shown in figure 6c. The as-achieved results of specific capacities for current densities of 1, 2, 3, 4, 5, 7, 10, and 20 A g^{-1}, respectively, at 2055.2, 1349, 1209.5, 1067,1034, 853.3, 705 and 210 C g^{-1} that tabulated in table 1. Based on the results, the $ZnCo_2S_4$/NF electrode material provides better reactions between the electrolyte and working electrode contacts, sufficient faradic reactions, and ease of charge storage and flight pathways. These values are also superior to those

obtained with other ternary metal sulfides such as $NiCo_2S_4$ measured in a similar potential window (table 2).

Table (1): The specific capacitance and capacity of the $ZnCo_2S_4$/NF sample at different current densities.

Current density (A g^{-1})	Specific capacitance (F g^{-1})	Specific capacity (C g^{-1})
1	1957.4	2055.2
2	1284.3	1349
3	1152	1209.5
4	1015	1067
5	985	1034
7	813	853.3
10	671	705
20	200	210

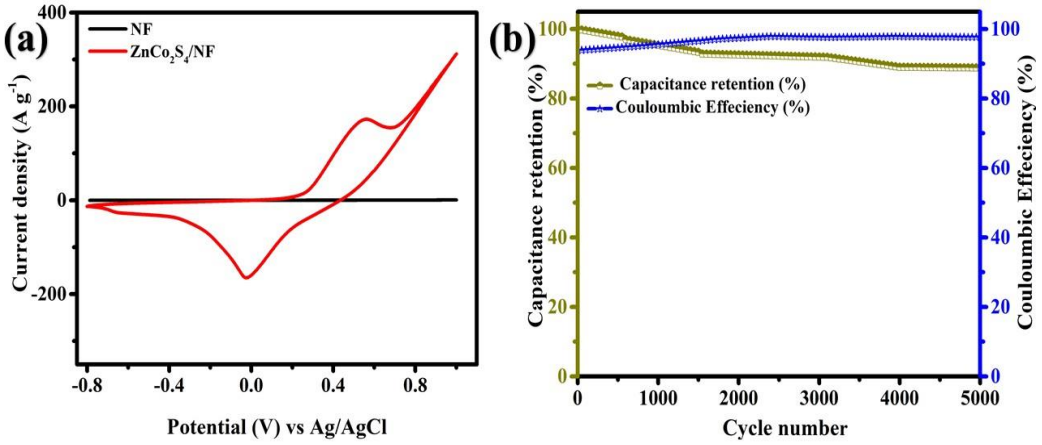

Fig. 7: (a) CV of $ZnCo_2S_4$/NF and pure NF at scan rate 10 mV s^{-1}, (b) Cycling stability of the $ZnCo_2S_4$ electrode at 10 A g^{-1} for 5000 cycles.

Table (2): Compares the performance of presently developed $ZnCo_2S_4$ with reported ternary metal sulfide supercapacitors in three-electrode configurations.

Electrode Materials	Capacitance (F g^{-1})	Current density (A g^{-1})	Electrolyte	Ref.
curtain-like zinc-cobalt sulfides	837 C g^{-1}	1 A g^{-1}	2 M KOH	[29]
$ZnCo_2S_4$ film	12082 C g^{-1}	1 A g^{-1}	3 M KOH	[35]
Carbon doped porous $MnCo_2S_4$ microcubes on Ni foam (solvothermal)	1892 C g^{-1}	5 A g^{-1}	3 M KOH	[41]
$Zn_{0.74}Co_{0.24}S_4$ nanosheets on nitrogen doped graphene/ carbon nanotube	486.2 F g^{-1}	2 A g^{-1}	1 M KOH	[25]
$NiCo_2S_4$ hollow hexagonal nanoplates	437 F g^{-1}	1 A g^{-1}	3 M KOH	[42]
2D $NiCo_2S_4$	1304 F g^{-1}	2 A g^{-1}	6 M KOH	[43]
$CuCo_2S_4$/CNT/graphene	504 F g^{-1}	10 A g^{-1}	6 M KOH	[44]
$ZnCo_2S_4$/ NF	2055 C g^{-1}	1 A g^{-1}	6 MKOH	This work

The Nyquist plots of the $ZnCo_2S_4$/NF electrode in the frequency range of 100 kHz to 0.01 Hz are shown in figure 6d before and after 5000 cycles. The equivalent circuit of the $ZnCo_2S_4$ electrode is shown in figure 6d, where R1 and Rct for Ohmic and charge-transfer resistance, respectively. W is the Warburg impedance, and C1 is the Faradaic capacitance [45, 46]. CPE is a constant phase element that represents double-layer capacitance. Note that the equivalent series resistance (ESR, which includes electrolyte resistance, internal electrode resistance, and electrode-to-electrolyte contact resistance) increased cycling from (0.8 to 2.53 Ω) after the cycling test, suggesting that Ohmic loss. The charge transfer resistance increased slightly (from 0.96 to 4.14 Ω), demonstrating that even after 5000 cycles, the $ZnCo_2S_4$ electrode maintains good electronic conductivity and capacitive performance. The near-vertical line in the low-frequency region indicates low electrolyte diffusion impedance. The downward slope difference between the vertical diffusion lines shows the outstanding capacitive performance of the electrode before and after 5000 charge/discharge cycles.

The CV curve area of the pure NF electrode is also displayed in figure 7a, revealing that NF exhibited negligible specific capacity [21]. Furthermore, the current intensity and CV area of the $ZnCo_2S_4$/NF electrode were higher than those of the NF electrode. Long cycle stability is essential to evaluate the battery-type SC electrode. As shown in figure 7b, the cycle stability of the $ZnCo_2S_4$/NF electrode was examined using 5000 GCD cycles at a current density of 10 A g^{-1}. The $ZnCo_2S_4$/NF electrode's coral reef-like structure demonstrated high cycling stability, 89.2 % after 5000 GCD cycles, indicating better cycling stability. In addition, the coulombic efficiency gradually improved after 5000 cycles, eventually reaching 98%. Furthermore, the electrochemical performances of hollow $ZnCo_2S_4$ core-shell nanospheres electrodes are superior to those previously reported metal sulfides electrode materials such as $NiCo_2S_4$ nanotube on Ni (76.1% after 1500 cycles) [47], Tube-like $NiCo_2S_4$ (75.9% after 5000 cycles) [48], Mushroom-like $CoNi_2S_4$ on Ni foam (75.8% after 3000 cycles)[49] and $CuCo_2S_4$ (80% after 2000 cycles) [50].

The symmetric battery supercapacitor hybrid was constructed with two $ZnCo_2S_4$/NF as positive and negative electrodes for more practical use. As illustrated in figure 8a, the suitable voltage window was evaluated by measuring CV curves with various voltage windows. The fast current enhancements were observed for each curve in the high potential region. However, the increased current is smaller for the curve with the potential window of 1.5 V. The rapid increase in current may be ascribed to the aqueous electrolyte's typical water oxidation process. Different scan rates (5- 100 mV s^{-1}) were employed to test the CV curves with the optimized voltage window of 1.5 V (figure 8b). Peak separation is small. Shape distortion is minimal, indicating that this device has a high reversibility window of 1.5 V. The rectangular shape of all CV curves is maintained without deviation until 100 mV s^{-1}, revealing the $ZnCo_2S_4$/NF// $ZnCo_2S_4$/NF device's superior stability characteristics. As shown in figure 8c, GCD analysis was done for the $ZnCo_2S_4$/NF// $ZnCo_2S_4$/NF device utilizing a constant potential window of 0 to 1.5 V and current densities ranging from 1 to 10 A g^{-1}. The device's specific capacities values were estimated at various current densities using equation (2) and shown in figure 8d, and at current densities of 1 A g^{-1}, it delivered 188 C g^{-1} specific capacity.

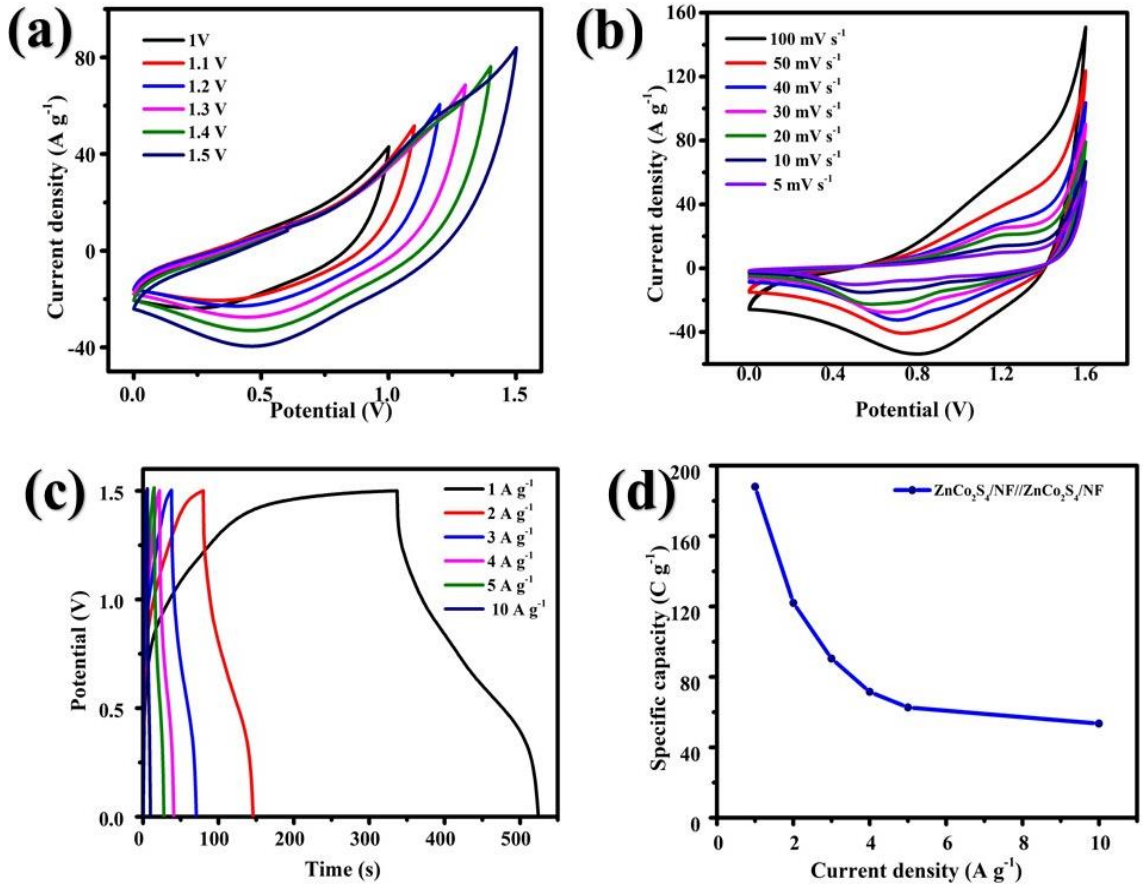

Fig. 8: CV curves at different voltage ranges from 1.0 to 1.5 V at 20 mV s^{-1} of $ZnCo_2S_4$/NF// $ZnCo_2S_4$/NF, (b) CV curves at different scan rates from 5 to 100 mV s^{-1} with a voltage window 0 to 1.5 V, of $ZnCo_2S_4$/NF// $ZnCo_2S_4$/NF (c) GCD curve for different current density ranging from 1 to 10 A g^{-1} with a voltage window of 0 to 1.5 V of $ZnCo_2S_4$/NF// $ZnCo_2S_4$/NF, and (d) specific capacities at different current densities of $ZnCo_2S_4$/NF// $ZnCo_2S_4$/NF.

The calculated specific capacities are 188, 122,90.4, 71.5, 62.7, and 53.46 C g^{-1} at different current densities from 1 to 10 A g^{-1}, as shown in figure 8d. The specific capacities of the $ZnCo_2S_4$/NF//$ZnCo_2S_4$/NF device was higher than the previously published work based on $ZnCo_2S_4$ and their composites such as $ZnCo_2S_4$//AC (160 C g^{-1} at 1 A g^{-1}) [35], $ZnCo_2S_4$/$ZnCo_2O_4$//CNT (130 F g^{-1} at 1 A g^{-1}) [51], $Zn_{0.76}Co_{0.24}S$/NGN/CNTs//NGN/CNTs (specific capacity 150.5 and 84.4 F g^{-1} at current density 0.5, 20 A g^{-1} respectively) [25] and other ternary metal sulfides based hybrid cells like, $MnCo_2S_4$//rGO (~88 F g^{-1} at1 A g^{-1}) [52], $NiCo_2S_4$/Co_9S_8//AC [53], $NiCo_2S_4$ NSs//AC (~72 F g^{-1} at 1.25 A g^{-1}) [54], porous $NiCo_2S_4$ NSs//AC (~80 F g^{-1} at ~3.6 A g^{-1}) [43], $NiCo_2S_4$ NBs//AC (~88 F g^{-1} at ~0.2 A g^{-1}) [55] , $NiCo_2S_4$/Co_9S_8//AC (107 F g^{-1} at 0.2 A g^{-1}) [53]. The EIS and its equivalent circuit in figures 9a and 9b, respectively, show the change in ESR of the device before and after the durability test. After 6,000 cycles, ESR increased from 0.38 Ω to 1.2 Ω, indicating the improved contact between electrode materials and electrolytes.

The Ragone plot of the symmetric device is displayed in figure 9c, which is plotted between specific energy and specific power factors using equations (3) and (4). The symmetric device provides the energy and power densities of 39.1 Wh kg^{-1} / 1637 W kg^{-1} at a current density of 1 A g^{-1}, respectively. In addition, the device attained 11.3 Wh kg^{-1} / 19278.8 W kg^{-1} of energy and power density at a current density of 10 A g^{-1}, respectively. These results superior to previously reported based on similar metal sulfide, such as Zn–Co–S/NF//AC/NF (31.9 Wh kg^{-1} at 850.0 W kg^{-1}) [28], $Zn_{0.76}Co_{0.24}S$/CFP (carbon fiber papers)//AC (9.59 Wh kg^{-1} at 750 W kg^{-1}) [56], $Co_3S_4/CoMo_2S_4$//AC (33.1 Wh kg^{-1} at 850 W kg^{-1}) [57], $NiCo_2S_4$//AC (28.3 Wh kg^{-1} at 245 W kg^{-1}) [58] and other devices shown in figure 9c [56, 57, 59-63]. The cyclic stability of the device was evaluated by GCD analysis as shown in figure 9d, utilizing an input current density of 20 A g^{-1} for 6000 continuous cycles. After 6000 cycles, the hybrid symmetric supercapacitor device retains 93.9 % of its capacitance and 100 % coulombic efficiency. This study confirmed that the $ZnCo_2S_4$/NF with nanocoral reef-like structure could meet the current demands of battery-type supercapacitor applications.

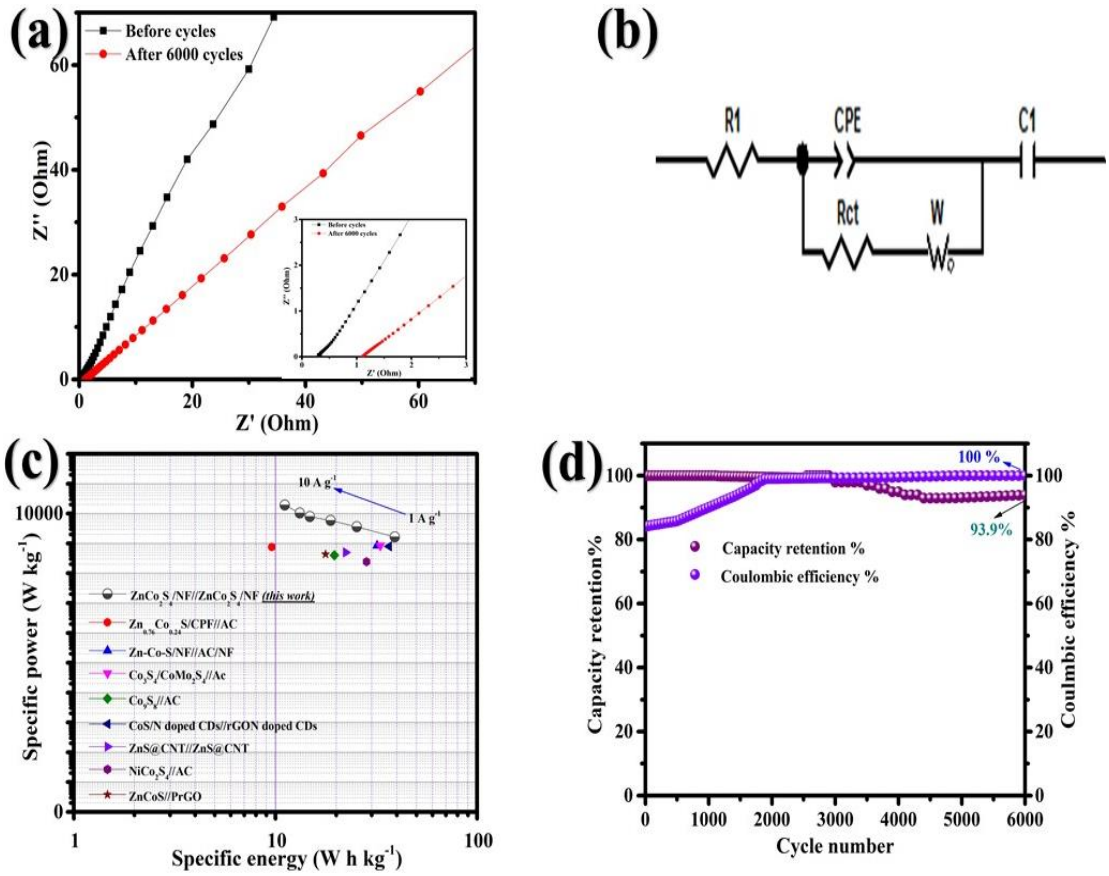

Fig. 9: (a) Ragone plot of $ZnCo_2S_4$/NF//$ZnCo_2S_4$/NF and comparison with other previous reports, (b) EIS curves of the $ZnCo_2S_4$/NF//$ZnCo_2S_4$/NF before and after 6000 cycles,(c) Equivalent circuit of $ZnCo_2S_4$/NF//$ZnCo_2S_4$/NF, and (d) cycling stability of $ZnCo_2S_4$/NF//$ZnCo_2S_4$/NF at 20 A g^{-1} through 5000 cycles.

4. CONCLUSIONS

A facile two-step hydrothermal approach was used to construct the $ZnCo_2S_4$ nanostructures that resemble coral reefs on NF. At a current density of 1 A g^{-1}, the $ZnCo_2S_4$ coral reef electrode displayed a maximum specific capacity of 2055.2 C g^{-1}. Likewise, the electrode revealed cyclic stability with 89.2 % capacity retention and 98 % coulombic efficiency after 5000 cycles. Furthermore, the battery-type symmetric $ZnCo_2S_4$/NF//$ZnCo_2S_4$/NF device delivered exceptional specific energy of 39.1 Wh kg^{-1} at a specific power of 1637 W kg^{-1} at a current density of 1 A g^{-1}, excellent cycling stability of 93.3 % after 6000 cycles, and remarkable coulombic efficiency of 100%. According to the findings, the nanocoral reef-like $ZnCo_2S_4$/NF structure is a great candidate for electrodes used in electrochemical energy storage applications.

Acknowledgement

The authors are grateful to Ceramic laboratory, Metallurgy Department, Nuclear Research Center, Egyptian Atomic Energy Authority, Tabbin Institute for Metallurgical Studies (TIMS), and Chemistry Department, Faculty of Science (Men), Al-Azhar University for providing facilities to carry out the work.

5. REFERENCES

[1] Wei, C., N. Zhan, J. Tao, S. Pang, L. Zhang, C. Cheng, and D. Zhang, "Synthesis of hierarchically porous $NiCo_2S_4$ core-shell hollow spheres via self-template route for high performance supercapacitors." Applied Surface Science, 2018. **453**: p. 288-296.

[2] Wei, C., R. Zhang, X. Zheng, Q. Ru, Q. Chen, C. Cui, G. Li, and D. Zhang, "Hierarchical porous $NiCo_2O_4$/CeO_2 hybrid materials for high performance supercapacitors." Inorganic Chemistry Frontiers, 2018. **5**(12): p. 3126-3134.

[3] Wei, C., Q. Chen, C. Cheng, R. Liu, Q. Zhang, and L. Zhang, "Mesoporous nickel cobalt manganese sulfide yolk–shell hollow spheres for high-performance electrochemical energy storage." Inorganic Chemistry Frontiers, 2019. **6**(7): p. 1851-1860.

[4] Wei, C., Q. Ru, X. Kang, H. Hou, C. Cheng, and D. Zhang, "Self-template synthesis of double shelled ZnS-$NiS_{1.97}$ hollow spheres for electrochemical energy storage." Applied Surface Science, 2018. **435**: p. 993-1001.

[5] Kulurumotlakatla, D.K., A.K. Yedluri, and H.-J. Kim, "Hierarchical $NiCo_2S_4$ nanostructure as highly efficient electrode material for high-performance supercapacitor applications." Journal of Energy Storage, 2020. **31**: p. 101619.

[6] Liu, P., Y. Sui, F. Wei, J. Qi, Q. Meng, Y. Ren, and Y. He, "Facile synthesis of $CoNi_2S_4$ nanoparticles grown on carbon fiber cloth for supercapacitor application." Journal of Materials Science: Materials in Electronics, 2019. **30**(21): p. 19077-19086.

[7] Huang, F., R. Meng, Y. Sui, F. Wei, J. Qi, Q. Meng, and Y. He, "One-step hydrothermal synthesis of a CoS_2@MoS_2 nanocomposite for high-performance supercapacitors." Journal of Alloys and Compounds, 2018. **742**: p. 844-851.

[8] Maier, M.A., R. Suresh Babu, D.M. Sampaio, and A.L.F. de Barros, "Binder-free polyaniline interconnected metal hexacyanoferrates nanocomposites (Metal = Ni, Co) on carbon fibers for flexible supercapacitors." Journal of Materials Science: Materials in Electronics, 2017. **28**(23): p. 17405-17413.

[9] Babu, R.S., A.L.F. de Barros, M. de Almeida Maier, D. da Motta Sampaio, J. Balamurugan, and J.H. Lee, "Novel polyaniline/manganese hexacyanoferrate

nanoparticles on carbon fiber as binder-free electrode for flexible supercapacitors." Composites Part B: Engineering, 2018. **143**: p. 141-147.

[10] Zhu, Y., Q. Zong, Q. Zhang, H. Yang, W. Du, Q. Wang, J. Zhan, and H. Wang, "Ultra-long lifespan asymmetrical hybrid supercapacitor device based on hierarchical NiCoP@C@LDHs electrode." Electrochimica Acta, 2020. **334**: p. 135589.

[11] Guan, B.Y., L. Yu, X. Wang, S. Song, and X.W. Lou, "Formation of Onion-Like $NiCo_2$ S_4 Particles via Sequential Ion-Exchange for Hybrid Supercapacitors." Adv Mater, 2017. **29**(6).

[12] Zhu, J., L. Wei, Q. Liu, and X. Kong, "Room-temperature preparation of amorphous CuNi-hybrid nanorod array as a fast battery-type electrode for high performance supercapacitor." Materials Chemistry and Physics, 2020. **247**: p. 122786.

[13] Guo, C., M. Yin, C. Wu, J. Li, C. Sun, C. Jia, T. Li, L. Hou, and Y. Wei, "Highly Stable Gully-Network Co_3O_4 Nanowire Arrays as Battery-Type Electrode for Outstanding Supercapacitor Performance." 2018. **6**.

[14] Attia, S.Y., S.G. Mohamed, Y.F. Barakat, H.H. Hassan, and W.A. Zoubi, "Supercapacitor electrode materials: addressing challenges in mechanism and charge storage" Reviews in Inorganic Chemistry." 2022. **42**(1): p. 53-88.

[15] El-Hout, S.I., S.Y. Attia, S.G. Mohamed, and S.M. Abdelbasir, "From waste to value-added products: Evaluation of activated carbon generated from leather waste for supercapacitor applications." Journal of Environmental Management, 2022. **304**: p. 114222.

[16] Huang, Y., A. Buffa, H. Deng, S. Sarkar, Y. Ouyang, X. Jiao, Q. Hao, and D. Mandler, "Ultrafine $Ni(OH)_2$ nanoplatelets grown on 3D graphene hydrogel fabricated by electrochemical exfoliation for high-performance battery-type asymmetric supercapacitor applications." Journal of Power Sources, 2019. **439**: p. 227046.

[17] Chou, S.-H., L.-Y. Lin, and Y.-H. Chiu, "Pulse reverse electrodeposited nickel cobalt sulfide nanosheets on Ni foam as battery-type electrode for battery supercapacitor hybrids." Journal of Energy Storage, 2019. **25**: p. 100903.

[18] Ranganatha, S. and N. Munichandraiah, "Solvothermal synthesis of mesoporous NiCoP for high performance electrochemical supercapacitors." Materials Chemistry and Physics, 2019. **224**: p. 124-128.

[19] Ahmed, S.Y., S.G. Mohamed, S.Y. Attia, Y.F. Barakat, M.A. Shoeib, and N.S. Tantawy, "High electrochemical energy-storage performance promoted by SnSe nanorods anchored on rGO nanosheets." Journal of Electroanalytical Chemistry, 2021. **883**: p. 115063.

[20] Kulkarni, P., S.K. Nataraj, R.G. Balakrishna, D.H. Nagaraju, and M.V. Reddy, "Nanostructured binary and ternary metal sulfides: synthesis methods and their application in energy conversion and storage devices." J. Mater. Chem. A, 2017. **5**(42): p. 22040-22094.

[21] Elsaid, M.A.M., A.A. Hassan, S.G. Mohamed, A.Z. Sayed, A.M. Ashmawy, and A.F. Waheed, "Synthesis and electrochemical performance of porous $FeCo_2S_4$ nanorods as an electrode material for supercapacitor." Journal of Energy Storage, 2021. **44**: p. 103330.

[22] Wang, X., Q. Zhang, J. Sun, Z. Zhou, Q. Li, B. He, J. Zhao, W. Lu, C.-p. Wong, and Y. Yao, "Facile synthesis of hierarchical porous manganese nickel cobalt sulfide nanotube arrays with enhanced electrochemical performance for ultrahigh energy density fiber-shaped asymmetric supercapacitors." Journal of Materials Chemistry A, 2018. **6**(17): p. 8030-8038.

[23] Hu, W., R. Chen, W. Xie, L. Zou, N. Qin, and D. Bao, "$CoNi_{(2)}S_{(4)}$ nanosheet arrays supported on nickel foams with ultrahigh capacitance for aqueous asymmetric supercapacitor applications." ACS Appl Mater Interfaces, 2014. **6**(21): p. 19318-26.
[24] Zhang, P., B.Y. Guan, L. Yu, and X.W. Lou, "Formation of Double-Shelled Zinc–Cobalt Sulfide Dodecahedral Cages from Bimetallic Zeolitic Imidazolate Frameworks for Hybrid Supercapacitors." 2017. **56**(25): p. 7141-7145.
[25] Tong, H., W. Bai, S. Yue, Z. Gao, L. Lu, L. Shen, S. Dong, J. Zhu, J. He, and X. Zhang, "Zinc cobalt sulfide nanosheets grown on nitrogen-doped graphene/carbon nanotube film as a high-performance electrode for supercapacitors." Journal of Materials Chemistry A, 2016. **4**(29): p. 11256-11263.
[26] Xu, W., X. Cui, Z. Xie, G. Dietrich, and Y. Wang, "Three-Dimensional Coral-Like Structure Constructed of Carbon-Coated Interconnected Monocrystalline SnO_2 Nanoparticles with Improved Lithium-Storage Properties." ChemElectroChem, 2016. **3**(7): p. 1098-1106.
[27] Liu, G., B. Wang, L. Wang, T. Liu, T. Gao, and D. Wang, "Facile controlled synthesis of a hierarchical porous nanocoral-like Co_3S_4 electrode for high-performance supercapacitors." RSC Advances, 2016. **6**(59): p. 54076-54086.
[28] Tao, K., X. Han, Q. Cheng, Y. Yang, Z. Yang, Q. Ma, and L. Han, "A Zinc Cobalt Sulfide Nanosheet Array Derived from a 2D Bimetallic Metal–Organic Frameworks for High-Performance Supercapacitors." 2018. **24**(48): p. 12584-12591.
[29] Xu, L., Y. Xi, X. Sun, P. Zhao, F. Zhu, J. Yin, L. Chen, J. Hu, and X. Li, "Hierarchically novel bead-curtain-like zinc-cobalt sulfides arrays toward high energy density hybrid supercapacitors via morphology engineering." Journal of Power Sources, 2021. **489**: p. 229535.
[30] Chen, Y.M., Z. Li, and X.W. Lou, "General Formation of $M_{(x)}Co_{(3-x)}S_4$ (M=Ni, Mn, Zn) Hollow Tubular Structures for Hybrid Supercapacitors." Angew Chem Int Ed Engl, 2015. **54**(36): p. 10521-4.
[31] Jiang, J., Y. Sun, Y. Chen, X. Hu, L. Zhu, H. Chen, and S. Han, "One-step synthesis of nickel cobalt sulfide nanostructure for high-performance supercapacitor." Journal of Materials Science, 2019. **54**(18): p. 11936-11950.
[32] Hussain, I., D. Mohapatra, G. Dhakal, C. Lamiel, M.S. Sayed, S. Sahoo, S.G. Mohamed, J.S. Kim, Y.R. Lee, and J.-J. Shim, "Uniform growth of ZnS nanoflakes for high-performance supercapacitor applications." Journal of Energy Storage, 2021. **36**: p. 102408.
[33] Geioushy, R.A., S.Y. Attia, S.G. Mohamed, R. A. A, and O.A. Fouad, "Polyvinylpyrrolidone and freeze drying-assisted growth of an α-$Ni(OH)_2$/reduced graphene oxide hybrid structure as a superior electrode material for supercapacitors." New Journal of Chemistry, 2021. **45**(22): p. 10012-10020.
[34] Yang, P. and W. Mai, "Flexible solid-state electrochemical supercapacitors." Nano Energy, 2014. **8**: p. 274-290.
[35] Atin Pramanik, S.M., Tanumoy Dhawa, Monjoy Sreemany, and S. Mahanty, "High faradaic charge storage in ZnCo2S4 film on Ni-foam with a hetero-dimensional microstructure for hybrid supercapacitor." Materials Today Energy, 2018. **9**: p. 416-427.
[36] Yang, Z., X. Zhu, K. Wang, G. Ma, H. Cheng, and F. Xu, "Preparation of $NiCo_2S_4$ flaky arrays on Ni foam as binder-free supercapacitor electrode." Applied Surface Science, 2015. **347**: p. 690-695.

[37] Yu, J., C. Lv, L. Zhao, L. Zhang, Z. Wang, and Q. Liu, "Reverse Microemulsion-Assisted Synthesis of $NiCo_2S_4$ Nanoflakes Supported on Nickel Foam for Electrochemical Overall Water Splitting." 2018. **5**(7): p. 1701396.
[38] Tao, K., Y. Gong, and J. Lin, "Epitaxial grown self-supporting $NiSe/Ni_3S_2/Ni_{12}P_5$ vertical nanofiber arrays on Ni foam for high performance supercapacitor: Matched exposed facets and re-distribution of electron density." Nano Energy, 2019. **55**: p. 65-81.
[39] Attia, S.Y., Y.F. Barakat, H.H. Hassan, and S.G. Mohamed, "A single-step synthesis and direct growth of microspheres containing the nanoflakes-like structure of $Zn_{0.76}Co_{0.24}S$ as a high-performance electrode for supercapacitors." Journal of Energy Storage, 2020. **29**: p. 101349.
[40] Wang, Y., C. Xiang, Y. Zou, F. Xu, L. Sun, and J. Zhang, "Three-dimensional polypyrrole-enhanced flower-like $ZnCo_2S_4$ nanoclusters used as advanced electrodes for supercapacitors." Journal of Energy Storage, 2021. **41**: p. 102838.
[41] Pramanik, A., S. Maiti, M. Sreemany, and S. Mahanty, "Carbon Doped $MnCo_2S_4$ Microcubes Grown on Ni foam as High Energy Density Faradaic Electrode." Electrochimica Acta, 2016. **213**: p. 672-679.
[42] Pu, J., F. Cui, S. Chu, T. Wang, E. Sheng, and Z. Wang, "Preparation and Electrochemical Characterization of Hollow Hexagonal $NiCo_2S_4$ Nanoplates as Pseudocapacitor Materials." ACS Sustainable Chemistry & Engineering, 2014. **2**(4): p. 809-815.
[43] Li, X., Q. Li, Y. Wu, M. Rui, and H. Zeng, "Two-Dimensional, Porous Nickel-Cobalt Sulfide for High-Performance Asymmetric Supercapacitors." ACS Appl Mater Interfaces, 2015. **7**(34): p. 19316-23.
[44] Shen, J., J. Tang, P. Dong, Z. Zhang, J. Ji, R. Baines, and M. Ye, "Construction of three-dimensional $CuCo_2S_4$/CNT/graphene nanocomposite for high performance supercapacitors." RSC Advances, 2016. **6**(16): p. 13456-13460.
[45] Qi, J., D. Wang, Z. Zhang, R. Hu, Y. Sui, Y. He, Q. Meng, and F. Wei, "Enhanced performance of mesoporous $NiCo_2S_4$ nanosheets fibre-shaped electrode for supercapacitor." 2021. **16**(4): p. 263-267.
[46] Mola, B.A., G. Mani, M.R. Pallavolu, N.R. Reddy, N.S. Alsaiari, F.M. Alzahrani, K.M. Katubi, Y. Noh, S.K. Jilcha, H.-J. Kim, and Y.A. Kumar, "Ni foam conductive substrate supported interwoven $ZnCo_2S_4$ nanowires with highly enhanced performances for supercapacitors." Journal of Energy Storage, 2021. **44**: p. 103417.
[47] Fu, W., C. Zhao, W. Han, Y. Liu, H. Zhao, Y. Ma, and E. Xie, "Cobalt sulfide nanosheets coated on $NiCo_2S_4$ nanotube arrays as electrode materials for high-performance supercapacitors." Journal of Materials Chemistry A, 2015. **3**(19): p. 10492-10497.
[48] Zhang, Y., M. Ma, J. Yang, C. Sun, H. Su, W. Huang, and X. Dong, "Shape-controlled synthesis of $NiCo_2S_4$ and their charge storage characteristics in supercapacitors." Nanoscale, 2014. **6**(16): p. 9824-30.
[49] Mei, L., T. Yang, C. Xu, M. Zhang, L. Chen, Q. Li, and T. Wang, "Hierarchical mushroom-like $CoNi_2S_4$ arrays as a novel electrode material for supercapacitors." Nano Energy, 2014. **3**: p. 36-45.
[50] Tang, J., Y. Ge, J. Shen, and M. Ye, "Facile synthesis of $CuCo_2S_4$ as a novel electrode material for ultrahigh supercapacitor performance." Chem Commun (Camb), 2016. **52**(7): p. 1509-12.

[51] Wang, X., P. Wu, Z. Zhao, L. Sun, Q. Deng, Z. Yin, and X. Chen, "Construction of flower-like $ZnCo_2S_4/ZnCo_2O_4$ arrays on Ni foam for high-performance asymmetric supercapacitors." Journal of Materials Science: Materials in Electronics, 2020. **31**(6): p. 4895-4904.

[52] Liu, S. and S.C. Jun, "Hierarchical manganese cobalt sulfide core–shell nanostructures for high-performance asymmetric supercapacitors." Journal of Power Sources, 2017. **342**: p. 629-637.

[53] Hou, L., Y. Shi, S. Zhu, M. Rehan, G. Pang, X. Zhang, and C. Yuan, "Hollow mesoporous hetero-$NiCo_2S_4/Co_9S_8$ submicro-spindles: unusual formation and excellent pseudocapacitance towards hybrid supercapacitors." Journal of Materials Chemistry A, 2017. **5**(1): p. 133-144.

[54] Wu, Z., X. Pu, X. Ji, Y. Zhu, M. Jing, Q. Chen, and F. Jiao, "High Energy Density Asymmetric Supercapacitors From Mesoporous $NiCo_2S_4$ Nanosheets." Electrochimica Acta, 2015. **174**: p. 238-245.

[55] Hou, L., H. Hua, R. Bao, Z. Chen, C. Yang, S. Zhu, G. Pang, L. Tong, C. Yuan, and X. Zhang, "Anion-Exchange Formation of Hollow $NiCo_2S_4$ Nanoboxes from Mesocrystalline Nickel Cobalt Carbonate Nanocubes towards Enhanced Pseudocapacitive Properties." 2016. **81**(6): p. 557-563.

[56] Zhang, M., Y. Sui, X. Yuan, J. Qi, F. Wei, Q. Meng, Y. He, Y. Ren, Z. Sun, and J. Liu, "Controllable $Zn_{0.76}Co_{0.24}S$ Nanoflower Arrays Grown on Carbon Fiber Papers for High-Performance Supercapacitors." 2019. **14**(03): p. 1950030.

[57] Yang, X., H. Sun, P. Zan, L. Zhao, and J. Lian, "Growth of vertically aligned $Co_3S_4/CoMo_2S_4$ ultrathin nanosheets on reduced graphene oxide as a high-performance supercapacitor electrode." Journal of Materials Chemistry A, 2016. **4**(48): p. 18857-18867.

[58] Zhu, Y., Z. Wu, M. Jing, X. Yang, W. Song, and X. Ji, "Mesoporous $NiCo_2S_4$ nanoparticles as high-performance electrode materials for supercapacitors." Journal of Power Sources, 2015. **273**: p. 584-590.

[59] Zhang, Y., N. Cao, S. Szunerits, A. Addad, P. Roussel, and R. Boukherroub, "Fabrication of ZnCoS nanomaterial for high energy flexible asymmetric supercapacitors." Chemical Engineering Journal, 2019. **374**: p. 347-358.

[60] Ji, Z., N. Li, M. Xie, X. Shen, W. Dai, K. Liu, K. Xu, and G. Zhu, "High-performance hybrid supercapacitor realized by nitrogen-doped carbon dots modified cobalt sulfide and reduced graphene oxide." Electrochimica Acta, 2020. **334**: p. 135632.

[61] Yao, T., Y. Li, D. Liu, Y. Gu, S. Qin, X. Guo, H. Guo, Y. Ding, Q. Liu, Q. Chen, J. Li, and D. He, "High-performance free-standing capacitor electrodes of multilayered Co_9S_8 plates wrapped by carbonized poly(3,4-ethylenedioxythiophene):poly(styrene sulfonate)/reduced graphene oxide." Journal of Power Sources, 2018. **379**: p. 167-173.

[62] Okeil, S., J. Krausmann, I. Dönges, S. Pfleger, J. Engstler, and J.J. Schneider, "ZnS/ZnO@CNT and ZnS@CNT nanocomposites by gas phase conversion of ZnO@CNT. A systematic study of their photocatalytic properties." Dalton Transactions, 2017. **46**(16): p. 5189-5201.

[63] Chen, H., J. Jiang, L. Zhang, H. Wan, T. Qi, and D. Xia, "Highly conductive $NiCo_2S_4$ urchin-like nanostructures for high-rate pseudocapacitors." Nanoscale, 2013. **5**(19): p. 8879-8883.